Acta Crystallographica Section D
Biological Crystallography
ISSN 0907-4449

The effect of deuteration on protein structure: a high-resolution comparison of hydrogenous and perdeuterated haloalkane dehalogenase

Xuying Liu,[a] B. Leif Hanson,[a] Paul Langan[b] and Ronald E. Viola[a]*

[a]Department of Chemistry, University of Toledo, Toledo, OH 43606, USA, and [b]Bioscience Division, Los Alamos National Laboratory, Los Alamos, NM 87544, USA

Correspondence e-mail: ron.viola@utoledo.edu

Received 27 April 2007
Accepted 31 July 2007

Haloalkane dehalogenase from *Xanthobacter autotrophicus* (*Xa*DHL) was overexpressed under different isotopic conditions to produce fully hydrogenous (h-*Xa*DHL) and perdeuterated (d-*Xa*DHL) enzyme forms. Deuterium atoms at labile positions were allowed to back-exchange during purification and hydrogenous solutions were used for crystallization. Optimal crystals of h-*Xa*DHL and d-*Xa*DHL were obtained under different pH conditions (pH 6.0 and 4.6, respectively) but had similar $P2_12_12$ unit cells. X-ray diffraction data were refined to 1.53 Å (h-*Xa*DHL) and 1.55 Å (d-*Xa*DHL) with excellent overall statistics. The conformations of h-*Xa*DHL and d-*Xa*DHL are similar, with slightly altered surface regions because of different packing environments, and h-*Xa*DHL is found to have a more hydrophobic core than d-*Xa*DHL. The active site of h-*Xa*DHL is similar to those of previously determined structures, but the active site of d-*Xa*DHL unexpectedly has some crucial differences. Asp124, the primary nucleophile in the hydrolysis of haloalkane substrates, is displaced from its position in h-*Xa*DHL and rotates to form a hydrogen bond with His289. As a consequence, the water molecule proposed to function as the nucleophile in the next catalytic step is excluded from the active site. This is the first observation of this unusual active-site configuration, which is obtained as a result of perdeuteration that decreases the hydrophobicity of the enzyme, therefore shifting the optimal pH of crystallization. This d-*Xa*DHL structure is likely to represent the termination state of the catalytic reaction and provides an explanation for the acid inhibition of *Xa*DHL. These results underline the importance of carefully verifying the assumption that isotopic substitution does not produce significant structural changes in protein structures.

1. Introduction

Haloalkane dehalogenases are key enzymes in the degradation of a broad range of haloalkanes, converting them to alcohols by hydrolytic cleavage of the carbon–halogen bond. The 35 kDa enzyme from *Xanthobacter autotrophicus* GJ10 (*Xa*DHL) is one of four enzymes involved (together with a second dehydrogenase, an aldehyde dehydrogenase and haloalkanoate dehalogenase) in the catabolic pathway of 1,2-dichloroethane, conferring on the bacterium the ability to grow using this substrate as the sole carbon source (Janssen *et al.*, 1985). 1,2-Dichloroethane is a colorless organic liquid that is widely utilized in plastic, rubber and synthetic textile fiber manufacturing and as a solvent of resins, cosmetics and drugs. The Environmental Protection Agency has found that 1,2-dichloroethane can potentially cause central nervous

© 2007 International Union of Crystallography
Printed in Denmark – all rights reserved

system disorders and produce adverse lung, kidney and liver circulatory effects when people are exposed to greater than 5 p.p.b. for even short periods of time. It has been estimated that approximately 10% of the large quantities of 1,2-dichloroethane used in industrial processes is lost to the environment every year, providing ample prospects for exposure. As a potential bioremediation candidate, *Xa*DHL is under consideration for use in cleaning contaminated soil and ground water rather than treatment with microbial *Xanthobacter autotrophicus* itself (Stucki & Thuer, 1995). However, this practical application of *Xa*DHL will require protein engineering to improve its catalytic efficiency, broaden its substrate specificity (Schanstra *et al.*, 1996) and overcome the inhibition by acid as the reaction proceeds.

*Xa*DHL has been studied extensively by X-ray crystallography. The folding of its backbone into a typical α/β-hydrolase fold and an α-helical cap, with the active site buried between these two domains in an internal cavity, has been examined from medium resolution (2.4 Å; Janssen *et al.*, 1985) to very high resolution (1.15 Å; Ridder *et al.*, 1999). The catalytic cavity is mainly hydrophobic (containing Trp125, Phe128, Leu262 and Leu263 from the α/β-hydrolase domain), with three hydrophilic catalytic residues (Asp124, Asp260 and His289) at the bottom. The cavity is further isolated from solvent by the hydrophobic α-helical cap (contributing Phe164, Phe172, Trp175, Phe222, Pro223 and Val226). In addition to these crystallographic studies, numerous biochemical studies of *Xa*DHL have contributed to the development of a putative mechanism for its catalytic activity (Damborsky & Koca, 1999; Holloway *et al.*, 1998; Pries *et al.*, 1994; Schindler *et al.*, 1999). However, uncertainties remain in the details of halide binding, the protonation states of the catalytic residues, the mechanism of hydrogen transfer during catalysis and the origin of acid inhibition. In order to resolve each of these key issues and also to provide a rational basis for protein engineering, the positions of H atoms in the active site must be established. Structural studies of *Xa*DHL by X-ray crystallography, even to very high resolution (Ridder *et al.*, 1999), have not provided the locations of any of these critical H atoms.

The location of H atoms is essential for understanding the mechanisms of enzyme-catalyzed reactions, as well as for detailed studies of structure–function relationships in general in macromolecules. The vast majority of the macromolecular structures that have been determined use the diffraction of X-rays to locate atomic positions. X-rays interact with the electron field of atoms: the more electrons an atom has, the stronger its interaction. Unfortunately, H atoms, with only a single electron per atom, are almost invisible in the presence of heavier atoms. Even in an ultrahigh-resolution (0.66 Å) study of aldose reductase, Podjarny and coworkers found that only about half of all H atoms could be located (Howard *et al.*, 2004). In contrast, neutrons are scattered mainly from the nuclei of atoms and H atoms interact with neutrons almost as well as C and O atoms. This means that in principle H-atom positions can be determined in macromolecules by neutron crystal diffraction even at modest resolutions.

One of the limitations of using neutron crystallography to locate hydrogen is that in addition to scattering neutrons coherently, hydrogen also scatters neutrons incoherently. With hydrogen accounting for up to half of the atoms in proteins, this incoherent scattering can contribute towards a large scattering background that limits the observation of weaker reflections. In addition, the negative scattering length of hydrogen means that it appears as a negative peak in nuclear density maps and will cancel the positive scattering length of covalently bound atoms at medium resolutions, reducing the effective scattering power of the crystal and making it difficult to interpret nuclear density maps. These effects, together with the relatively weak flux of available neutron beams from most sources, have limited the application of neutron protein crystallography to proteins that can be crystallized to volumes of >0.3 mm^3 (Blum *et al.*, 2007).

Replacing hydrogen with deuterium can minimize each of these limitations and make neutron crystallographic studies possible for an expanded number of proteins. D atoms have a strong positive scattering length and cause little incoherent scattering. D atoms therefore appear as strong positive peaks in nuclear density maps and replacing hydrogen with deuterium can enhance the signal-to-noise ratio of weaker reflections and increase the effective scattering power of the crystal, especially at medium resolution. The labile H atoms in proteins (those bound to N and O atoms) can be substituted by deuterium simply by growing or soaking existing crystals in D_2O mother liquor, with the extent of substitution depending on accessibility and local protein dynamics. However, labile H atoms typically account for only about 25% of the total hydrogen in a protein. To substitute the remaining H atoms and obtain a fully deuterated (perdeuterated) protein requires expressing the gene of interest in an organism that is adapted for growth in deuterated media. The effectiveness of perdeuteration in improving neutron crystallography was first demonstrated with myoglobin (Shu *et al.*, 2000). More recently, perdeuteration has been shown to make neutron crystallography possible with crystal volumes as small as 0.1 mm^3 (Hazemann *et al.*, 2005).

This paper describes the successful production of perdeuterated *Xa*DHL and its characterization by MALDI mass spectrometry and X-ray crystallography. A comparison of the X-ray structures of the hydrogenous enzyme, h-*Xa*DHL, and the perdeuterated enzyme, d-*Xa*DHL, is presented. The differences observed in the active-site structures of these enzyme forms provide insights into the catalytic mechanism and the acid inhibition of *Xa*DHL, as well as general implications for the use of perdeuteration in the study of enzyme mechanisms.

2. Experimental procedures

2.1. Expression and purification of hydrogenous and perdeuterated haloalkane dehalogenase

In order to allow a direct comparison of the effect of perdeuteration on *Xa*DHL, both d-*Xa*DHL and h-*Xa*DHL

were expressed from the same plasmid (provided by Dr John Schindler while on the staff at LANL). Expression of h-*Xa*DHL has been described previously (Schanstra *et al.*, 1993). Expression of d-*Xa*DHL was similar except that a culture medium developed at Los Alamos, designated Altone, was used. Altone is based on a culture medium developed by Stone *et al.* (1987) but without glucose or glycerol supplements and with the addition of a number of micro-elements (2% *Scenedesmus obliquus* hydrolyzate plus the following salts per litre of D_2O: 1.1 g ND_4Cl, 100 mg $MgSO_4$, 3.0 g KD_2PO_4, 3.2 g Na_2DPO_4, 2 mg $CaCl_2$, 2 mg $FeCl_3$, 2.8 mg D_3BO_3, 900 µg $MnCl_2.4D_2O$, 80 µg $CaSO_4.5D_2O$, 150 µg $Na_2MoO_4.2D_2O$, 220 µg $ZnSO_4.7D_2O$). A 5 ml starting culture was grown overnight using hydrogenous LB broth in a shaker at 310 K and 250 rev min^{-1}. The starting culture was then used to inoculate two 500 ml cultures of Altone media in 2 l baffled flasks. Growth was monitored by measuring the optical density at 600 nm. After 7.5 h, when the OD_{600} had reached ∼0.2, the culture was induced with 0.5 ml of 1 *M* IPTG per 500 ml culture and the incubator temperature was reduced to 303 K. After an additional 15 h, when the OD_{600} was 2.2 (Fig. 1*a*), 13.5 g of cell paste was harvested by centrifugation at 3000*g* for 30 min and was stored at 193 K. The supernatant taken from the centrifuge tubes was retained for D_2O recycling.

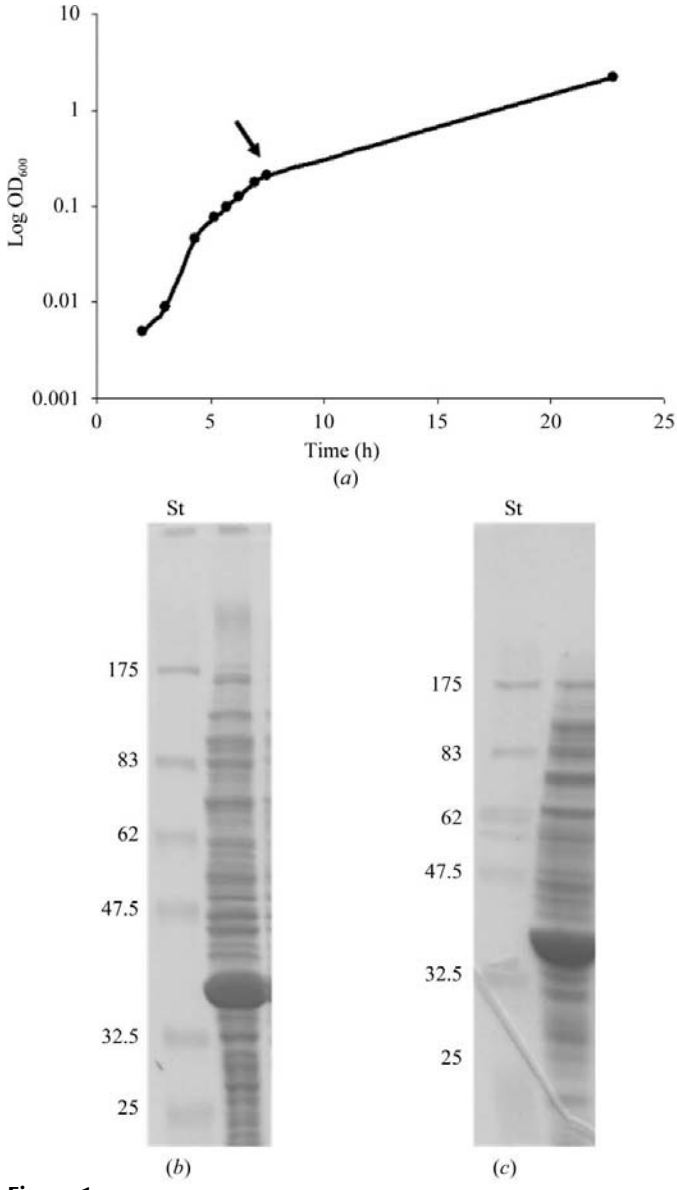

Figure 1
(*a*) Perdeuterated *Xa*DHL growth curve. The *y* axis is shown on a logarithmic scale, with an arrow indicating the point of induction with IPTG. (*b*) and (*c*) SDS–PAGE of hydrogenous *Xa*DHL (*b*) and perdeuterated *Xa*DHL (*c*) cell extracts. In both gels, lane St contains molecular-weight markers (kDa).

For both enzyme forms, the high levels of expression allowed an abbreviated purification procedure in which pure protein was obtained using a simple two-step protocol: ammonium sulfate fractionation followed by anion-exchange chromatography. Both hydrogenated and perdeuterated cells were thawed and suspended in H_2O medium containing 20 m*M* Tris–HCl pH 7.5, 1 m*M* EDTA, 1 m*M* BME (TEB buffer) at a ratio of 0.1 g of cells per millilitre of buffer and the cell suspension was disrupted by sonication on ice. The cell lysis was centrifuged to remove cellular debris. A stepwise salt fractionation was employed by slow addition of finely powdered ammonium sulfate first to 50% and then to 80% saturation with stirring for 1 h at 277 K and with centrifugation at each step. The precipitate between 50% and 80% ammonium sulfate saturation containing most of the *Xa*DHL activity was collected by centrifugation and resuspended in 20 m*M* MES pH 6.0 with 1 m*M* EDTA and 1 m*M* BME (MEB buffer) and then dialyzed for 18 h against several changes of the same buffer at 277 K. The dialyzed enzyme solution was applied onto a Source 30Q anion-exchange column equilibrated with MEB buffer. *Xa*DHL eluted from the column at approximately 150 m*M* ammonium sulfate in an ascending linear gradient from 0 to 800 m*M* ammonium sulfate in MEB buffer. The active fractions were pooled and dialyzed against 4 l MEB buffer. The expression and purification of both h-*Xa*DHL (Fig. 1*b*) and d-*Xa*DHL (Fig. 1*c*) were analyzed by SDS–PAGE, with a final yield of 43 mg pure h-*Xa*DHL and 28 mg d-*Xa*DHL per litre of growth medium. Enzyme solutions were concentrated with Amicon Ultra centrifugal filter devices (Millipore Co.) and the concentration of each solution was determined by a Bradford dye-binding assay (Bradford, 1976). While it was found that h-*Xa*DHL could easily be concentrated above 30 mg ml^{-1} and remain soluble, d-*Xa*DHL had decreased solubility and started to precipitate when the concentration approached 9 mg ml^{-1}.

2.2. Crystallization and X-ray data collection

The crystallization of both h-*Xa*DHL and d-*Xa*DHL was carried out at 293 K using the hanging-drop vapor-diffusion method [4 µl hanging drops consisting of 2 µl protein solution (12 µg) and 2 µl reservoir solution suspended over 600 µl reservoir solution]. H_2O, not D_2O, was used in all solutions. The optimal crystallization conditions, in particular pH, for growing large crystals differed slightly for h-*Xa*DHL and d-*Xa*DHL. Crystals of h-*Xa*DHL were obtained with a reservoir consisting of 2.4 *M* ammonium sulfate in 100 m*M*

MES pH 6.0 and grew to maximum dimensions of 0.50 × 0.45 × 0.20 mm over several days (Fig. 2*b*). Crystals of d-*Xa*DHL were obtained with a reservoir consisting of 2.6 *M* ammonium sulfate in 100 m*M* sodium acetate pH 4.6 and grew to approximately 0.30 × 0.25 × 0.10 mm over a similar time period (Fig. 2*a*). The h-*Xa*DHL crystals were cryoprotected with 30% PEG 6000, 20% glycerol and 100 m*M* MES buffer pH 6.0, while the d-*Xa*DHL crystals were cryoprotected with the same components except that sodium acetate buffer pH 4.6 was used instead of MES buffer pH 6.0. Crystals were flash-frozen in liquid nitrogen. A 1.53 Å diffraction data set for h-*Xa*DHL was collected in-house using our FR-E diffractometer with an R-AXIS IV image-plate detector. These crystals belonged to space group $P2_12_12$, with unit-cell parameters $a = 41.2$, $b = 72.2$, $c = 92.7$ Å. The d-*Xa*DHL crystal diffraction data were collected to 1.55 Å resolution using the same instrument and correspond to the same space group $P2_12_12$, with slightly different unit-cell parameters of $a = 40.0$, $b = 71.1$, $c = 94.4$ Å. Both data sets were processed and scaled with *CrystalClear* (Table 1).

Table 1
Data-collection and model-refinement statistics.

Values in parentheses are for the highest resolution shell.

	Hydrogenous XaDHL	Perdeuterated XaDHL
Data-collection statistics		
Temperature (K)	100	100
Space group	$P2_12_12$	$P2_12_12$
Unit-cell parameters (Å)	$a = 41.2$, $b = 72.2$, $c = 92.7$	$a = 40.0$, $b = 71.1$, $c = 94.4$
Resolution (Å)	37.62–1.53 (1.59–1.53)	28.76–1.55 (1.62–1.55)
Total No. of reflections	222104	145629
No. of unique reflections	36268	41347
Completeness (%)	85.4 (23.3)	96.1 (71.0)
R_{merge}	0.055 (0.257)	0.077 (0.352)
Output $\langle I/\sigma(I)\rangle$	17.5 (3.1)	9.4 (1.8)
Refinement statistics		
Resolution range (Å)	37.62–1.53	28.76–1.55
R_{work}/R_{free} (%)	15.6/18.4	18.8/22.6
No. of residues	308	308
No. of waters	499	350
R.m.s. deviations		
Bond lengths (Å)	0.009	0.009
Bond angles (°)	1.195	1.172
Coordinate ESU based on R/R_{free} (Å)	0.092/0.088	0.149/0.102
DPI†	0.0843	0.0996
Average *B* values (Å^2)		
Protein atoms	23.2	27.4
Waters	43.9	42.8
Ramachandran plot, residues in (%)		
Most favorable region	89.1	88.7
Additional favorable region	10.4	11.3
Generously allowed region	0.4	0.0
Disallowed region	0.0	0.0

† Dispersion precision index calculated by *REFMAC*5.

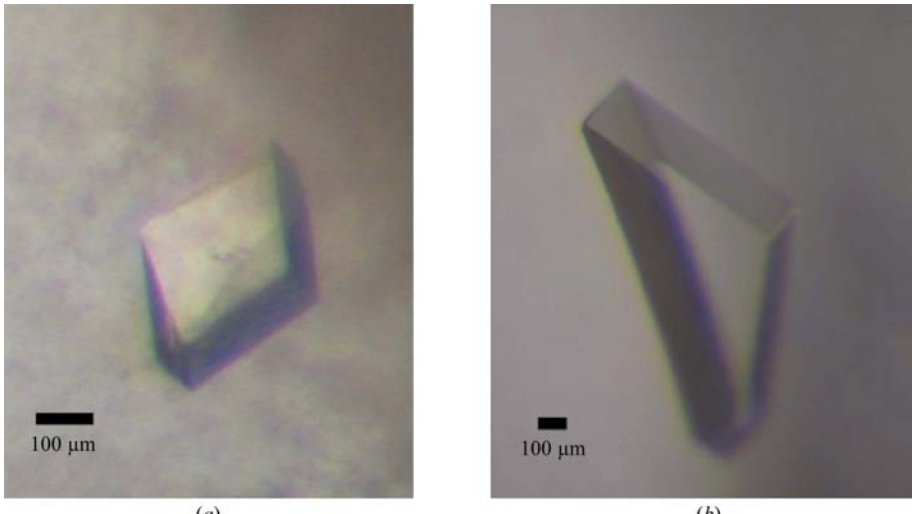

Figure 2
Typical crystals of haloalkane dehalogenase used for X-ray diffraction studies. (*a*) Perdeuterated *Xa*DHL; (*b*) hydrogenous *Xa*DHL.

2.3. Structure determination and model refinement

*REFMAC*5 (Murshudov *et al.*, 1997) was used for structural refinement and *Coot* (Emsley & Cowtan, 2004) was used for model building and fitting. The published 1.19 Å structure (PDB code 1b6g; Ridder *et al.*, 1999) was used as the starting model for molecular replacement. The deviation of the unit-cell parameters from those of the target structure was within 2%, allowing rigid-body refinement to be used directly to position the molecule more accurately in the cell. This was followed by restrained refinement in combination with *ARP* (Lamzin & Wilson, 1993) to automatically model and update the solvent structure and then manual evaluation of each water molecule in *Coot*. The final values of R_{work} and R_{free} for d-*Xa*DHL, which diffracted to a resolution of 1.55 Å, are 18.8% and 22.6%, respectively, and the final model consists of 308 amino acids and 350 water molecules. Most of the amino acids fit into the electron density quite well, with only a small number of surface-residue side chains lacking clear density. The final model is of excellent quality, with root-mean-square deviations (r.m.s.d.s) of 0.009 Å for bond lengths and 1.17° for bond angles. The final model of h-*Xa*DHL is of even higher quality and was refined with 499 water molecules to 1.53 Å with values of 15.6% and 18.4% for R_{work} and R_{free}, respectively. The coordination error, as estimated by B_{eq}, is represented in Fig. 3.

The average B_{eq} for the h-*Xa*DHL and d-*Xa*DHL polypeptide chains are 23.2 and 27.4 Å^2, respectively. The structure-refinement statistics for both structures are reported in Table 1.

3. Results

3.1. Deuteration of haloalkane dehalogenase

We used the biological deuteration laboratory that supports the Protein Crystallography Station (PCS) at Los Alamos Neutron Scattering Center (Langan *et al.*, 2004) for the perdeuteration of *Xa*DHL as a first step towards neutron crystallographic studies. While straightforward in principle, protein-expression systems can be sensitive both to the replacement of H_2O by D_2O in the growth medium and to the exact amount and types of deuterated nutrients used and can also require lengthy adaptation periods before substantial growth is achieved. The biological deuteration laboratory uses an algae-based procedure for deuteration that is relatively inexpensive and efficient and does not require extensive adaptation. Many photosynthetic algae are capable of autotrophic growth in an inorganic environment using CO_2 as their sole carbon source. These organisms can be fully deuterated relatively inexpensively because D_2O is the only deuterium-containing compound required to support their growth (Katz & Crespi, 1966). Bacteria can also be grown on D_2O, but they require the addition of deuterated metabolites in order to obtain high levels of deuteration. Mass production of the deuterated green algae *S. obliquus* can be used as an inexpensive source of deuterated metabolites, in particular amino acids, carbohydrates and fatty acids, for the subsequent cultivation of bacteria (Crespi & Katz, 1972). This approach is exploited at the biological deuteration laboratory in order to provide a facility for expressing large quantities of perdeuterated proteins in *Escherichia coli*.

MALDI mass spectrometry, which was carried out by the proteome-mapping service at the University of Michigan, was used to determine the deuteration level of d-*Xa*DHL which had been back-exchanged with deuterated medium after purification in hydrogenous buffers. By comparing the mass differences between h-*Xa*DHL and d-*Xa*DHL samples with the calculated number of H/D atoms, the level of substitution was determined to be 100%; the measured number of deuterons in d-*Xa*DHL was 2442 ± 25 deuterons, which slightly exceeds the calculated number of 2396 H atoms in the enzyme, indicating complete deuteration.

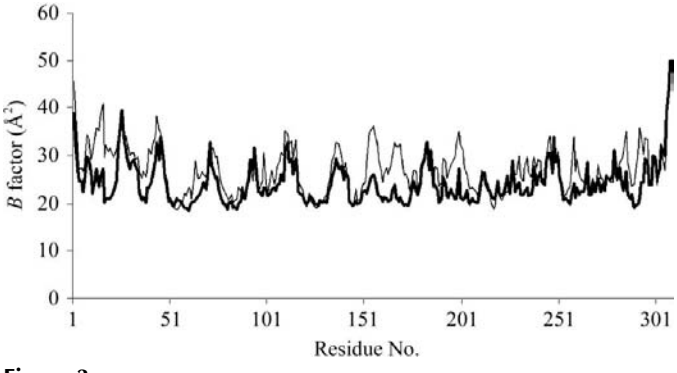

Figure 3
Average *B* values for each residue of hydrogenous (thick line) and perdeuterated (thin line) *Xa*DHL, as calculated using the *CCP*4 program suite.

3.2. Overall structure comparison of h-*Xa*DHL and d-*Xa*DHL

Alignment of the refined structures of h-*Xa*DHL and d-*Xa*DHL demonstrates that the overall conformations of these enzyme forms are almost identical, with an average root-mean-square deviation (r.m.s.d.) value of 0.24 Å. The C$^\alpha$ distances ($D_{C\alpha}$) between identical residues in the superimposed structures were used to identify any regions of deviation that may exist between the structures and the square of the C$^\alpha$ distance ($D_{C\alpha}^2$) was plotted *versus* residue number to enhance the visibility of these regions. This analysis identified four regions of significant deviation (labeled *A*–*D*) and five additional regions (labeled *e*–*i*) of smaller deviation (Fig. 4*a*). A mapping of these regions onto the enzyme structure reveals

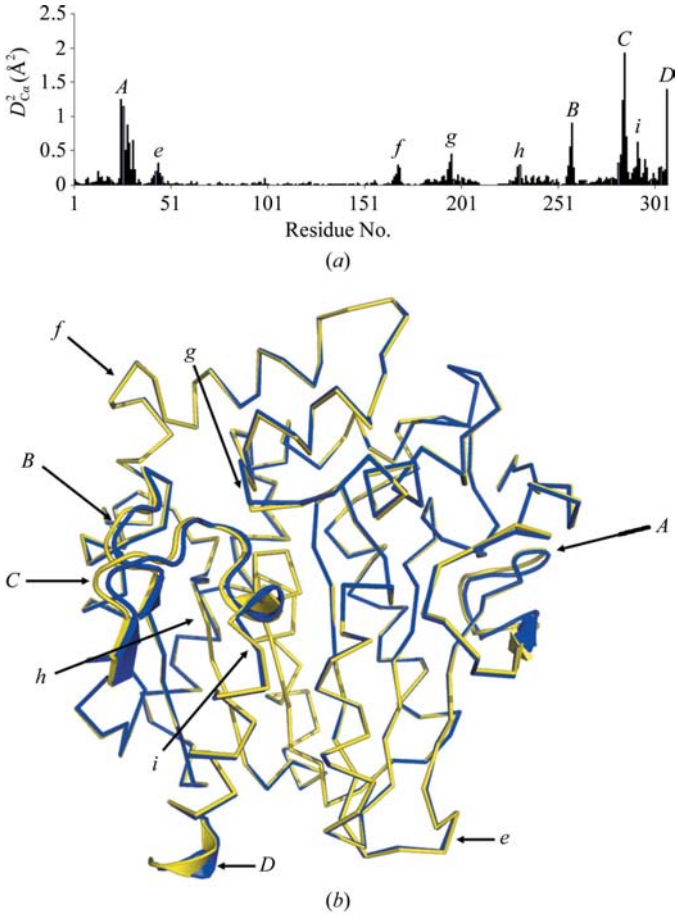

Figure 4
Overall structure comparison of hydrogenous *Xa*DHL and perdeuterated *Xa*DHL. (*a*) Square of the distance between the respective C$^\alpha$ atoms ($D_{C\alpha}^2$) *versus* residue-number plot, with the regions of maximum deviation labeled *A*–*D* and *e*–*i* (see text for explanation). (*b*) Overlay of hydrogenous *Xa*DHL (blue) and perdeuterated *Xa*DHL (yellow) structures generated and rendered with *PyMOL*, with the regions of deviation labeled corresponding to the peaks in (*a*).

that each of them is located on the surface of the protein (Fig. 4*b*). Region *D* corresponds to the disordered C-terminus of the enzyme. Analysis of the crystal lattice interfaces using the PISA (Protein Interfaces, Surfaces and Assemblies) server shows that regions *A*–*C* and *e*–*i* are each associated with flexible loops at protein interfaces which interact with ordered α-helical regions of adjacent protein molecules in the crystal lattice. h-*Xa*DHL has a slightly larger surface area (12 123 Å^2) than that of d-*Xa*DHL (12 085 Å^2). Consequently, in the comparable unit cells the crystal packing of h-*Xa*DHL is more compact, with a slightly larger contact area (3637 Å^2) compared with d-*Xa*DHL (3618 Å^2). It is most likely to be the differences in crystal packing between hydrogenous and perdeuterated *Xa*DHL that are responsible for the observed deviations in these regions, rather than any inherent conformational changes between the two enzyme forms.

3.3. Active-site comparison of h-*Xa*DHL and d-*Xa*DHL

If these surface loops account for the only differences between h-*Xa*DHL and d-*Xa*DHL, then our results would be consistent with earlier studies, which concluded that perdeuteration has a negligible effect on protein structure. However, the active site of d-*Xa*DHL differs crucially from that of h-*Xa*DHL in several structural details and is found in a configuration that has not been previously reported in any published structure of this enzyme. The active site of *Xa*DHL is located in the loop regions between the cap domain and the main domain and is characterized by relatively low *B* values. The residue side chains of d-*Xa*DHL and h-*Xa*DHL are aligned very well in these regions, with the largest deviation observed at the Leu62 side chain, which deviates by about 0.43 Å. However, the most striking differences are observed for the hydrophilic catalytic residues. Compared with its configuration in h-*Xa*DHL, a 20° rotation about χ_2 of Asp124 in d-*Xa*DHL causes C$^{\alpha}$ to move by 0.2 Å. This is propagated into a 0.95 Å movement of the side-chain carboxyl O atom towards His289, while His289 moves away from its position in the hydrogenated structure by 0.32 Å to allow formation of a hydrogen bond between His289 N$^{\varepsilon 2}$ and Asp124 O$^{\delta 1}$ (Fig. 5). As a consequence, the hydrolytic water molecule that is present in h-*Xa*DHL is not found in the active site in d-*Xa*DHL. Lowering the contouring of the $2F_o - F_c$ map to 0.7σ (Fig. 5*b*) still does not identify sufficient density to place a water molecule at this position. This particular water is a proposed nucleophile during catalysis and previous X-ray crystallographic studies have shown it to be particularly stable and well positioned, with a *B* value that is 1.6-fold lower than the average for the other water molecules. This structural difference, produced as a result of deuteration, is sufficient to convert *Xa*DHL into a catalytically inactive conformation.

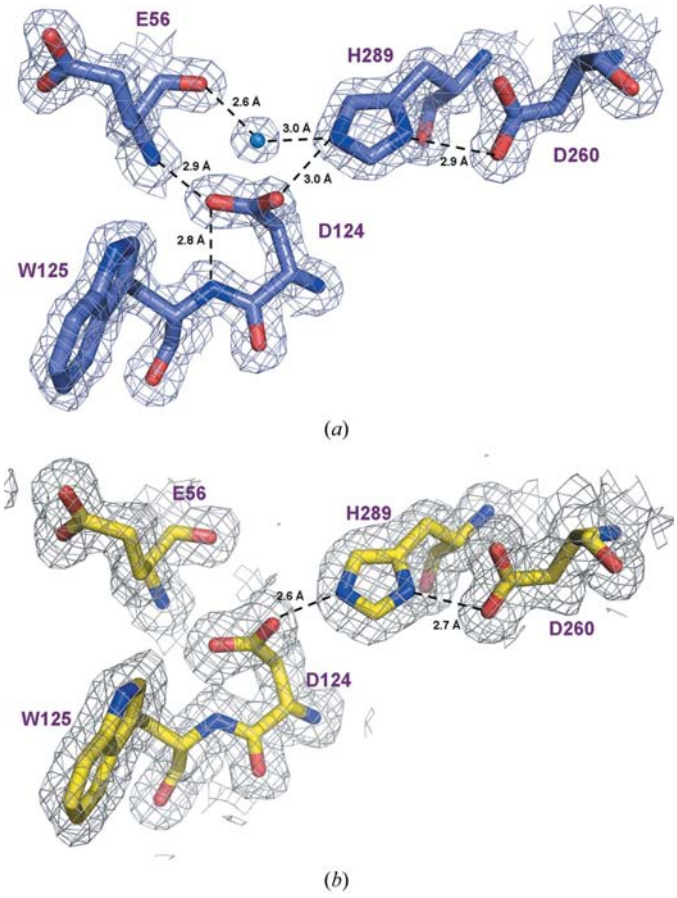

Figure 5
$2F_o - F_c$ electron-density (light blue) levels for the catalytic residues Asp124/His289/Asp260 of (*a*) hydrogenous *Xa*DHL contoured at 1.5σ (blue) and (*b*) perdeuterated *Xa*DHL contoured at 0.7σ (yellow). The figure was generated and rendered with *PyMOL*.

4. Discussion

4.1. Protein deuteration

While protein perdeuteration has been demonstrated to greatly enhance the neutron diffraction properties of crystals, the number of neutron structures that have resulted from use of this approach is still quite small (Hazemann *et al.*, 2005; Shu *et al.*, 2000). This is at least partly because the process of deuteration has been expensive and complex. The increased availability of deuterated metabolites and reagents, the development of robust protocols and access to central deuteration facilities has resulted in an increased use of perdeuteration as a first step towards neutron crystallographic studies (Artero *et al.*, 2005; Budayova-Spano *et al.*, 2006; Meilleur *et al.*, 2004; Tuominen *et al.*, 2004). We have successfully produced d-*Xa*DHL for neutron crystallographic studies at the PCS biological deuteration laboratory at Los Alamos National Laboratories using a new protocol that is relatively inexpensive, does not require extensive adaptation, produces high protein yields and results in a high level (∼100%) of H/D substitution.

4.2. Structural comparison of h-*Xa*DHL and d-*Xa*DHL

The expectation in the use of perdeuteration in neutron protein crystallography, particularly when studying enzyme mechanisms, is that hydrogenated and deuterated proteins will have virtually identical crystal structures. However, in the case of *Xa*DHL we have found some significant differences in

properties between d-*Xa*DHL and h-*Xa*DHL. d-*Xa*DHL has decreased solubility compared with h-*Xa*DHL, an effect of perdeuteration that has been reported previously and that has been proposed to arise from a reduction in folding stability (Brockwell *et al.*, 2001; Meilleur *et al.*, 2004). The best crystals of d-*Xa*DHL were obtained under more acidic conditions than those used to obtain crystals of h-*Xa*DHL, although the same precipitant was used in each case. Despite these differences, the crystals of both proteins have the same morphology and similar unit-cell parameters and their overall structures are similar, in agreement with previously reported comparisons of the crystal structures of hydrogenous and perdeuterated proteins (Artero *et al.*, 2005; Budayova-Spano *et al.*, 2006; Cooper *et al.*, 1998; Meilleur *et al.*, 2005). However, our detailed structural analysis demonstrates that there are some differences in the surface regions of d-*Xa*DHL and h-*Xa*DHL that can be associated with slightly different crystal-packing environments.

Some of these differences between d-*Xa*DHL and h-*Xa*DHL can be explained by the different properties of C—H and C—D groups. While d-*Xa*DHL was expressed with all of the H atoms replaced by deuterium, hydrogenous solutions were used during purification and crystallization and the labile deuterons in the protein were allowed to exchange back to protons. This approach was taken in order to study the effects of deuteration on the protein alone without involving D_2O/H_2O solvent effects. The chemical structures of d-*Xa*DHL and h-*Xa*DHL therefore differ only in their respective C—D and C—H bonding motifs. C—D bonds are known to be shorter than C—H bonds; because deuterium is twice the mass of hydrogen, the characteristic vibrations associated with a C—D bond are weaker than those associated with a C—H bond (Carey & Sundberg, 2000). As a consequence of their smaller volume, C—D bonds have reduced hydrophobicity compared with C—H bonds (Hattori *et al.*, 1965). Globular protein folding, though complicated, is primarily driven by the hydrophobicity of the nonpolar regions of amino-acid side chains (Dyson *et al.*, 2006) and therefore d-*Xa*DHL is expected to be somewhat less stable. This notion is supported by the identification of a hydrophobic core comprised of 43 mainly nonpolar solvent-inaccessible residues in h-*Xa*DHL, whereas only 39 such residues are present in the solvent-inaccessible core of d-*Xa*DHL. The requirement for more acidic solvent conditions for crystallization may be needed to compensate for the weaker hydrophobicity of d-*Xa*DHL, since the relative hydrophobicity of a protein will increase as a consequence of protonation at lower pH.

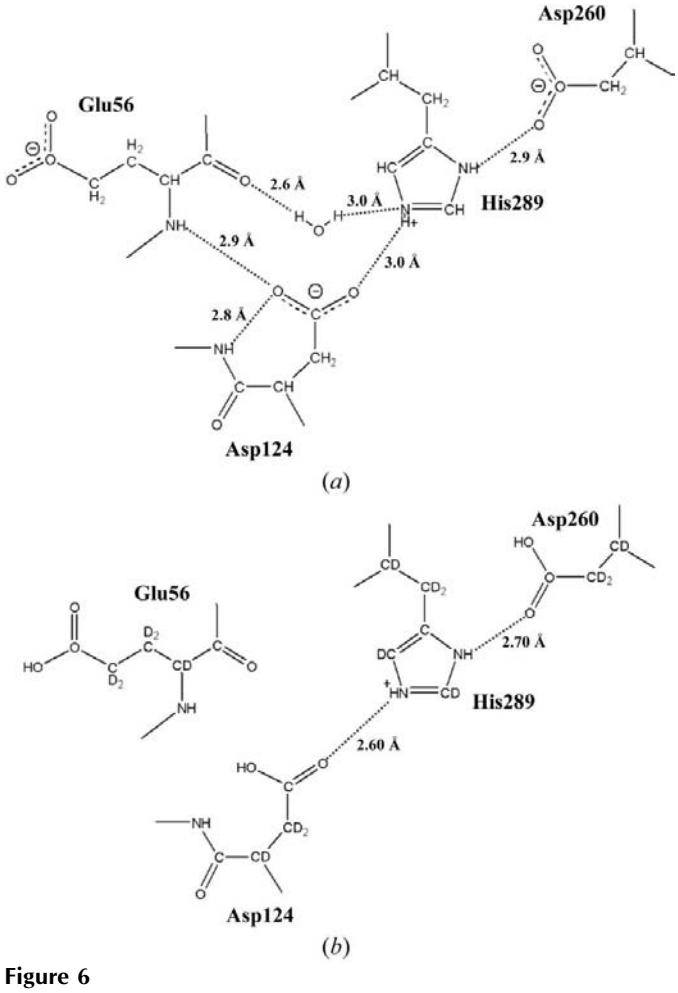

Figure 6
Proposed hydrogen-binding network in the catalytic cavity for (*a*) hydrogenous *Xa*DHL at pH 6.0 and (*b*) perdeuterated *Xa*DHL at pH 4.6. Hydrogen bonds are shown by dotted lines between the proton donors and acceptors.

4.3. Effect of pH on the *Xa*DHL structure

The observed differences between the catalytic sites of d-*Xa*DHL and h-*Xa*DHL can partly be explained by the increased acidity of the crystallization conditions for d-*Xa*DHL which is required to compensate for the decrease in protein hydrophobicity. However, perdeuteration is also expected to cause changes in the pK_a values of protein functional groups. Crystallographic studies at different pH values suggest that Asp124 $O^{\delta1}$ is responsible for nucleophilic attack on the C-1 atom of the substrate, forming an intermediate ester which is subsequently cleaved by a hydrolytic water (Verschueren, Seljee *et al.*, 1993; Verschueren, Franken *et al.*, 1993). At pH 6.2, well below the optimum for activity, His289 $N^{\varepsilon2}$ appears to be weakly hydrogen bonded to Asp124 $O^{\delta1}$, suggesting that the N atom is at least partially protonated. The structure of the active site of h-*Xa*DHL (at pH 6.0) is similar to that previously reported at pH 6.2 (Verschueren, Franken *et al.*, 1993). In particular, similar distances and angles are observed between His289 $N^{\varepsilon2}$ and Asp124 $O^{\delta1}$, suggesting that these atoms are weakly hydrogen bonded and therefore that His289 $N^{\varepsilon2}$ is protonated. However, given the estimated pK_a of 6.0 for His289 $N^{\varepsilon2}$, the existence of a hydrogen bond between this donor and acceptor at pH 6.0–6.2 is not clear. Asp124 is stabilized by two additional hydrogen bonds between Asp124 $O^{\delta2}$ and two backbone amide groups (from Asp124 and Glu56) and these hydrogen bonds may be more important in stabilizing the side-chain position of Asp124 than the putative interaction with His289. At pH 8.2, which is near the optimum for activity,

His289 $N^{\varepsilon 2}$ is proposed to be deprotonated and moves away from Asp124 by about 0.6 Å. This shift puts His289 in position to abstract a proton from the hydrolytic water, assisted by the concerted action of Asp260 coordinated to His289 $N^{\delta 1}$.

4.4. Role of nucleophilic water molecule

The crucial nucleophilic water in the active site of h-*Xa*DHL, as in previous reported structures of *Xa*DHL determined over a range of pH values, is in an ideal position (Fig. 5*a*) to donate a proton to His289 $N^{\varepsilon 2}$ suggesting, in contrast to the evidence presented above, that His289 $N^{\varepsilon 2}$ should be ionized for maximal activity. This active-site water also forms a hydrogen bond to the backbone carbonyl O atom of Glu56 in h-*Xa*DHL (Fig. 6*a*). However, the hydrolytic water is not present in the active site of d-*Xa*DHL determined at pH 4.6 (Fig. 5*b*). This was unexpected, since electron density for this hydrolytic water is still clearly present in a previously published structure of *Xa*DHL determined at pH 5.0 (Ridder *et al.*, 1999). It seems likely that the water molecule is excluded from the active site because of the formation of a strong hydrogen bond between His289 $N^{\varepsilon 2}$ and Asp124 $O^{\delta 1}$ (Fig. 5*b*). The water molecule would no longer have sufficient space or potential hydrogen-bonding partners in the strongly hydrophobic environment within the active site. Formation of this strong hydrogen bond requires the protonation of His289 $N^{\varepsilon 2}$. A reduction of 0.4 pH units (from 5.0 to 4.6) would make this protonation more likely; however, it is also possible that it is an increase in the pK_a values of His289 and Asp124 (from their predicted values of 6.0 and 4.4, respectively) owing to perdeuteration that favors the formation of this hydrogen bond. Replacing C—H bonds by C—D bonds in His289 and Asp124 will increase the electronegativity of His289 $N^{\varepsilon 2}$ and the carboxylate group of Asp124, thus raising their pK_a and the likelihood of their remaining protonation. Protonation of Asp124 would also disrupt the hydrogen bond accepted by Asp124 $O^{\delta 2}$ from the backbone amide group of Glu56, allowing Asp124 to swing towards His289 so that Asp124 $O^{\delta 2}$ can accept the hydrogen bond from His289 $N^{\varepsilon 2}$. Even if Asp124 does not become protonated at pH 4.6, it may be that the strong hydrogen bond between His289 $N^{\varepsilon 2}$ and Asp124 $O^{\delta 1}$ is energetically favored over the alternative hydrogen bonds that could be made to a water molecule and a backbone amide. Resolving these ambiguities by determining the exact location of H atoms in the active site of *Xa*DHL is the goal of the planned neutron crystallographic studies.

4.5. Mechanistic insights gained from deuteration

This arrangement of side chains found in the catalytic site of d-*Xa*DHL has not been observed before. It is well established that when *Xa*DHL hydrolyzes its haloalkane substrate it releases a proton. This catalytic reaction is sensitive to pH and its optimum reaction pH is around 8.2. As catalysis proceeds, more protons are generated and the catalytic environment will become more acidic. The measured reaction rate decreases and eventually becomes undetectable at very low pH. This new structural arrangement at the active site of d-*Xa*DHL provides a structural explanation for the reaction termination. Formation of a strong hydrogen bond between Asp124 and His289 excludes the nucleophilic water from the catalytic site. The catalytic site of d-*Xa*DHL, if Asp124 is not protonated, may represent the arrangement during catalysis after the covalent intermediate ester has been cleaved by the hydrolytic water, with His289 $N^{\varepsilon 2}$ retaining the proton abstracted from the nucleophilic water and the chloride product still bound in the active site. The chloride ion could then abstract the proton from His289 $N^{\varepsilon 2}$, breaking the hydrogen bond between His289 $N^{\varepsilon 2}$ and Asp124 $O^{\delta 1}$, leaving the active site and allowing another water in, thus regenerating the enzyme. As the local acidity of the environment increases, the need for the chloride ion to break the hydrogen bond between His289 $N^{\varepsilon 2}$ and Asp124 $O^{\delta 1}$ decreases and the strength of the hydrogen bond increases.

5. Conclusions

In the case of haloalkane dehydrogenase, structural evidence is presented showing that perdeuteration results in a decrease in protein hydrophobicity that lowers the pH required for crystallization. Together with an increase in the pK_a of catalytic residues, again owing to perdeuteration, this has led to the fortuitous observation of a completely new reaction-site motif. These results suggest that perdeuteration could be used in general to drive an active site towards a more acidic environment when crystallization is not possible with hydrogenous protein at low pH. The results of this study underline the importance of fully characterizing perdeuterated proteins using X-ray crystallography before their use in neutron crystallographic studies of enzyme mechanisms.

The authors thank Dr John Schindler for providing the plasmid containing the *Xa*DHL gene and Mary Jo Waltman for technical assistance in the production of *Xa*DHL in deuterated media. This work was supported by a National Science Foundation grant (466218) to BLH.

References

Artero, J.-B., Härtlein, M., McSweeney, S. & Timmins, P. (2005). *Acta Cryst.* D**61**, 1541–1549.
Blum, M. M., Koglin, A., Ruterjans, H., Schoenborn, B., Langan, P. & Chen, J. C. (2007). *Acta Cryst.* F**63**, 42–45.
Bradford, M. (1976). *Anal. Biochem.* **72**, 248–253.
Brockwell, D., Yu, L., Cooper, S., McCleland, S., Cooper, A., Attwood, D., Gaskell, S. J. & Barber, J. (2001). *Protein Sci.* **10**, 572–580.
Budayova-Spano, M., Fisher, S. Z., Dauvergne, M.-T., Agbandje-McKenna, M., Silverman, D. N., Myles, D. A. A. & McKenna, R. (2006). *Acta Cryst.* F**62**, 6–9.
Carey, F. A. & Sundberg, R. J. (2000). *Advanced Organic Chemistry*, 4th ed. Dordrecht: Kluwer Academic Publishers.
Cooper, S. J., Brockwell, D., Raftery, J., Attwood, D., Barber, J. & Helliwell, J. R. (1998). *Chem. Commun.* **10**, 1063–1064.
Crespi, H. L. & Katz, J. J. (1972). *Methods Enzymol.* **26**, 627–637.
Damborsky, J. & Koca, J. (1999). *Protein Eng.* **12**, 989–998.
Dyson, H. J., Wright, P. E. & Scheraga, H. A. (2006). *Proc. Natl Acad. Sci. USA*, **103**, 13057–13061.

Emsley, P. & Cowtan, K. (2004). *Acta Cryst.* D**60**, 2126–2132.
Hattori, A., Crespi, H. L. & Katz, J. J. (1965). *Biochemistry*, **4**, 1213–1225.
Hazemann, I., Dauvergne, M. T., Blakeley, M. P., Meilleur, F., Haertlein, M., Van Dorsselaer, A., Mitschler, A., Myles, D. A. A. & Podjarny, A. (2005). *Acta Cryst.* D**61**, 1413–1417.
Holloway, P., Knoke, K. L., Trevors, J. T. & Lee, H. (1998). *Biotechnol. Bioeng.* **59**, 520–523.
Howard, E. I., Sanishvili, R., Cachau, R. E., Mitschler, A., Chevrier, B., Barth, P., Lamour, V., Van Zandt, M., Sibley, E., Bon, C., Moras, D., Schneider, T. R., Joachimiak, A. & Podjarny, A. (2004). *Proteins*, **55**, 805–813.
Janssen, D. B., Scheper, A., Dijkhuizen, L. & Witholt, B. (1985). *Appl. Environ. Microbiol.* **49**, 673–677.
Katz, J. J. & Crespi, H. L. (1966). *Science*, **151**, 1187–1194.
Lamzin, V. S. & Wilson, K. S. (1993). *Acta Cryst.* D**49**, 129–147.
Langan, P., Greene, G. & Schoenborn, B. P. (2004). *J. Appl. Cryst.* **37**, 24–31.
Meilleur, F., Contzen, J., Myles, D. A. A. & Jung, C. (2004). *Biochemistry*, **43**, 8744–8753.
Meilleur, F., Dauvergne, M.-T., Schlichting, I. & Myles, D. A. A. (2005). *Acta Cryst.* D**61**, 539–544.
Murshudov, G. N., Vagin, A. A. & Dodson, E. J. (1997). *Acta Cryst.* D**53**, 240–255.
Pries, F., Kingma, J., Pentenga, M., Van Pouderoyen, G., Jeronimus-Stratingh, C. M., Bruins, A. P. & Janssen, D. B. (1994). *Biochemistry*, **33**, 1242–1247.
Ridder, I. S., Rozeboom, H. J. & Dijkstra, B. W. (1999). *Acta Cryst.* D**55**, 1273–1290.
Schanstra, J. P., Ridder, I. S., Heimeriks, G. J., Rink, R., Poelarends, G. J., Kalk, K. H., Dijkstra, B. W. & Janssen, D. B. (1996). *Biochemistry*, **35**, 13186–13195.
Schanstra, J. P., Rink, R., Pries, F. & Janssen, D. B. (1993). *Protein Expr. Purif.* **4**, 479–489.
Schindler, J. F., Naranjo, P. A., Honaberger, D. A., Chang, C. H., Brainard, J. R., Vanderberg, L. A. & Unkefer, C. J. (1999). *Biochemistry*, **38**, 5772–5778.
Shu, F., Ramakrishnan, V. & Schoenborn, B. P. (2000). *Proc. Natl Acad. Sci. USA*, **97**, 3872–3877.
Stone, D. B., Curmi, P. M. & Mendelson, R. A. (1987). *Methods Cell Biol.* **28**, 215–229.
Stucki, G. & Thuer, M. (1995). *Environ. Sci. Technol.* **29**, 2339–2345.
Tuominen, V. U., Myles, D. A. A., Dauvergne, M.-T., Lahti, R., Heikinheimo, P. & Goldman, A. (2004). *Acta Cryst.* D**60**, 606–609.
Verschueren, K. H. G., Franken, S. M., Rozeboom, H. J., Kalk, K. H. & Dijkstra, B. W. (1993). *J. Mol. Biol.* **232**, 856–872.
Verschueren, K. H. G., Seljee, F., Rozeboom, H. J., Kalk, K. H. & Dijkstra, B. W. (1993). *Nature (London)*, **363**, 693–698.